







Cite this: *Chem. Sci.*, 2023, 14, 12366

All publication charges for this article have been paid for by the Royal Society of Chemistry

Mechanistic studies of isomeric [2]rotaxanes consisting of two different tetrathiafulvalene units reveal that the movement of cyclobis(paraquat-*p*-phenylene) can be controlled†

Sofie K. Jensen,  Mathias S. Neumann,  Rikke Frederiksen, 
Mathias L. Skavenborg,  Mads C. Larsen,  Stinne E. Wessel
and Jan O. Jeppesen *

Controlling the movement in artificial molecular machines is a key challenge that needs to be solved before their full potential can be harnessed. In this study, two isomeric tri-stable [2]rotaxanes **1**·4PF₆ and **2**·4PF₆ incorporating both a tetrathiafulvalene (TTF) and a monopyrrolotetrathiafulvalene (MPTTF) unit in the dumbbell component have been synthesised to measure the energy barriers when the tetracationic cyclobis(paraquat-*p*-phenylene) (CBPQT⁴⁺) ring moves across either a TTF²⁺ or an MPTTF²⁺ dication. By strategically exchanging one of the thiomethyl barriers on either the TTF unit or the MPTTF unit with the bulkier thioethyl group, the movement of the CBPQT⁴⁺ ring in **1**⁴⁺ and **2**⁴⁺ can be controlled to take place in only one direction upon tetra-oxidation. Cyclic voltammetry and ¹H NMR spectroscopy were used to investigate the switching mechanism and it was found that upon tetra-oxidation of **1**⁴⁺ and **2**⁴⁺, the CBPQT⁴⁺ ring moves first to a position where it is located between the TTF²⁺ and MPTTF²⁺ dications producing high-energy co-conformations which slowly interconvert into thermodynamically more stable co-conformations. The kinetics of the movement occurring in the tetra-oxidised [2]rotaxanes **1**⁸⁺ and **2**⁸⁺ were studied at different temperatures allowing the free energy of the transition state, when CBPQT⁴⁺ moves across TTF²⁺ (21.5 kcal mol^{−1}) and MPTTF²⁺ (20.3 kcal mol^{−1}) at 298 K, to be determined. These results demonstrate for the first time that the combination of a TTF and an MPTTF unit can be used to induce directional movement of the CBPQT⁴⁺ ring in molecular machines with a 90% efficiency.

Received 22nd August 2023
Accepted 23rd October 2023

DOI: 10.1039/d3sc04408d

rsc.li/chemical-science

Introduction

Life relies on motion induced by a variety of molecular machines. Nature uses these machines to regulate chemical processes, ensuring that a specific sequence of actions is followed, and that work performed in one process is not cancelled in the next. Inspired by naturally occurring molecular machines, such as the ATP synthase¹ or the kinesin motor protein,² there is a great current interest in designing and synthesising artificial molecular machines (AMMs)³ that mimic biomachines/biomotors and use their underlying mechanistic principles to create systems capable of performing rotary and linear movements at the molecular level.^{2b,3,4,5} Large amplitude motion in AMMs, similar to what can be observed in biomachines, can be achieved by conformational or

configurational changes in covalently bonded molecules^{5g,6} or in supramolecular architectures.^{5h,7} In both cases, control of directionality is of paramount importance if rectified motion, such as unidirectional linear motion or unidirectional circum-rotational motion in AMMs should be realised. In the latter case, significant progress toward this end has been made possible as a consequence of the formation/discovery of the mechanical bond.⁸ Directional movements in mechanically interlocked molecules (MIMs), such as catenanes⁹ and rotaxanes,⁹ can be obtained either through systems that rely on an energy ratchet mechanism^{3,10} or on an information ratchet mechanism.^{3,10b} The information ratchet operates continuously in a non-equilibrium steady state, while the energy ratchet operates in a stepwise manner. In both cases, the key requirement is the ability to change both the thermodynamical distribution between two states and the kinetical interconversion between them, in order to obtain kinetic asymmetry.^{3,10b,11} Exemplary studies have shown (i) how simultaneous modification of recognition sites and covalently linked steric barriers can be used to create unidirectional movement in catenanes,^{7d}

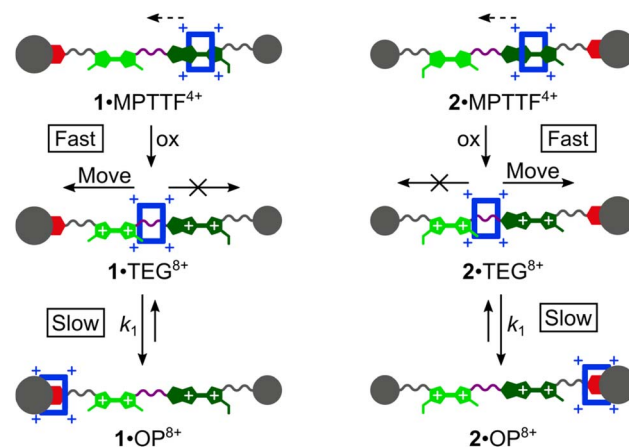
Department of Physics, Chemistry and Pharmacy, University of Southern Denmark, Campusvej 55, 5230 Odense, Denmark. E-mail: joj@sdu.dk

† Electronic supplementary information (ESI) available: Synthetic details and procedures with full characterisation, 1D and 2D NMR spectra and full description of kinetic experiments. See DOI: <https://doi.org/10.1039/d3sc04408d>

(ii) how an asymmetric set of steric and electrostatic barriers can be used to pump macrocycles across a linear axle¹² and latest (iii) how the introduction of asymmetry in a macrocycle can be used to control the directionality of the movement of the macrocycle on a symmetric dumbbell component in a [2]rotaxane.¹³ Mechanistic studies on AMMs, therefore, are essential if the next generation of AMMs with enhanced control of movement should be developed.

MIMs based on the tetracationic electron-accepting macrocycle cyclobis(paraquat-*p*-phenylene) (CBPQT⁴⁺) and the electron-donating tetrathiafulvalene (TTF) unit^{7c,14} have been used extensively for the construction of AMMs. TTF and many of its derivatives show a high binding with CBPQT⁴⁺ as a result of the formation of charge-transfer (CT) interactions between the electron-deficient bipyridinium moieties present in CBPQT⁴⁺ and the electron-rich TTF unit.¹⁵ By oxidising the TTF unit to the TTF radical cation (TTF^{•+}) or the TTF dication (TTF²⁺), the favourable CT interactions between TTF and CBPQT⁴⁺ are replaced by coulombic repulsion between TTF^{•+}/TTF²⁺ and the tetracationic CBPQT⁴⁺ ring, forcing CBPQT⁴⁺ to move away from the oxidised TTF unit.^{7c,15b} This motif has successfully been used as the switching gear in numerous redox-switchable [2]rotaxanes and [2]catenanes based on CBPQT⁴⁺ and TTF^{7a,c,14,16} and illustrates that the electroactive TTF unit can be used as a stimuli-controlled station for the CBPQT⁴⁺ ring. However, the symmetric nature of most TTF derivatives result in non-directional movement of CBPQT⁴⁺ away from the oxidised TTF unit, *i.e.* the encircling CBPQT⁴⁺ ring can leave the oxidised TTF unit in both directions with equal probability (Scheme S1a, ESI†). This problem can be circumvented if the monopyrroloTTF (MPTTF) unit is used as the electroactive component. On account of its non-symmetrical nature, the MPTTF unit can be used to induce directional movement of CBPQT⁴⁺ following its oxidation, since the combination of the thiomethyl (SMe) and the thioalkyl (SR) groups acts as a steric barrier that forces the CBPQT⁴⁺ ring to escape from the oxidised MPTTF unit in only one direction (Scheme S1b, ESI†), *i.e.* across the pyrrole moiety present in MPTTF.†

Most recently, some of us have discovered that TTF/MPTTF also can act as stimuli-induced electrostatic barriers for the movement of CBPQT⁴⁺. It was found that both the di-oxidised TTF²⁺ and MPTTF²⁺ dications can act as electrostatic barriers for the CBPQT⁴⁺ ring when both units are present in a tetra-stable [2]rotaxane.^{14d} Although it was not possible to quantify the size of the barriers when the CBPQT⁴⁺ ring moves across the di-oxidised units, it was found that the barrier for CBPQT⁴⁺ to move across the MPTTF²⁺ dication is about 0.5 kcal mol⁻¹ smaller than over the TTF²⁺ dication.^{14d} Later, we used a simple bistable [2]rotaxane as the platform to make a complete profiling of the energy landscape when the CBPQT⁴⁺ ring moves across an MPTTF²⁺ dication in both the forward and the backward directions and it was estimated that the Gibbs free energy of activations (ΔG^\ddagger) for these processes were 21.8 (forward) and 23.3 (backward) kcal mol⁻¹, respectively, in CD₃CN at 298 K.^{7e} However, no studies have so far been directed toward quantifying the barrier when CBPQT⁴⁺ moves across a TTF²⁺ dication, and more importantly, to quantify to which extent the



Scheme 1 Oxidation of the two isomeric [2]rotaxanes 1·MPTTF⁴⁺ and 2·MPTTF⁴⁺ producing initially 1·TEG⁸⁺ and 2·TEG⁸⁺, respectively, which subsequently in a slow and rate-limiting step converts into 1·OP⁸⁺ and 2·OP⁸⁺, respectively allowing the rate constants k_1 for the movement of CBPQT⁴⁺ (blue) from the TEG linker across either a TTF²⁺ (light green) or an MPTTF²⁺ (dark green) to the OP (red) unit to be determined. In 1·TEG⁸⁺ and 2·TEG⁸⁺, the movement of CBPQT⁴⁺ to the right and left, respectively, is rendered impossible by attachment of a large and bulky thioethyl (SEt) group to either the MPTTF²⁺ (1·TEG⁸⁺) or the TTF²⁺ (2·TEG⁸⁺) unit.

combination of an MPTTF and a TTF unit following their oxidations can be used to induce directional movement of the CBPQT⁴⁺ ring in MIMs. Toward this end, we have designed (Scheme 1) a set of isomeric [2]rotaxanes 1·MPTTF⁴⁺ and 2·MPTTF⁴⁺, incorporating both a TTF (light green) and an MPTTF (dark green) unit in the dumbbell component, that allow us to quantify the size of the energy barriers when the CBPQT⁴⁺ ring (blue) moves across either a TTF²⁺ or an MPTTF²⁺ dication. By strategically exchanging one of the SMe barriers on either the TTF unit or the MPTTF unit with the much bulkier thioethyl (SEt) group, the movement of the CBPQT⁴⁺ ring can be isolated to take place in only one direction, on account of the fact¹⁷ that the combination of the SEt and the SR groups acts as a stopper for CBPQT⁴⁺. Following tetra-oxidation of 1·MPTTF⁴⁺ and 2·MPTTF⁴⁺, it was found that the CBPQT⁴⁺ ring moves in between the TTF²⁺ and MPTTF²⁺ dications producing 1·TEG⁸⁺ and 2·TEG⁸⁺, respectively. These two co-conformations represent metastable states (out-of-equilibrium) of the oxidised [2]rotaxanes 1⁸⁺ and 2⁸⁺, which slowly interconvert into the thermodynamically more stable co-conformations 1·OP⁸⁺ and 2·OP⁸⁺, respectively, when CBPQT⁴⁺ moves across either the TTF²⁺ dication in 1⁸⁺ or the MPTTF²⁺ dication in 2⁸⁺. This observation allowed us to determine the rate constants (k_1) and associated ΔG^\ddagger values when CBPQT⁴⁺ moves across a TTF²⁺ or an MPTTF²⁺ dication and to elucidate the impact of the increased electrostatic repulsion present when the CBPQT⁴⁺ ring is located between two doubly oxidised units (*i.e.* TTF²⁺ and MPTTF²⁺).

Here, we describe (i) the template-directed synthesis and characterisation of two isomeric tri-stable [2]rotaxanes 1·4PF₆ and 2·4PF₆ (Fig. 1) in which the ring component is CBPQT⁴⁺ (blue) and the dumbbell component contains three potential



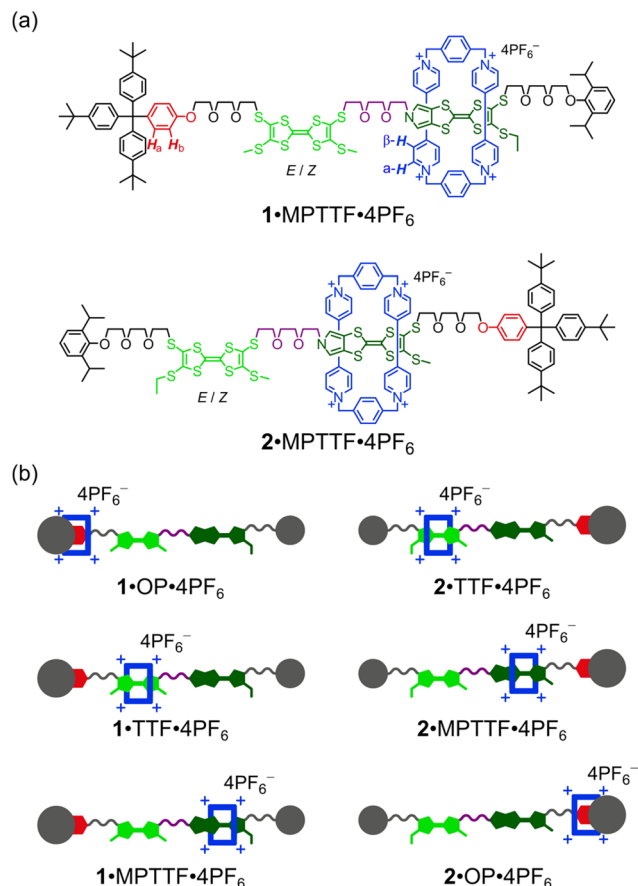


Fig. 1 (a) Molecular formulas of the tri-stable [2]rotaxanes **1**·4PF₆ and **2**·4PF₆ (only one translational isomer for each is shown). (b) Cartoon representations of the three possible translational isomers of **1**·4PF₆ and **2**·4PF₆, respectively (all translational isomers also exist as a mixture of E- and Z-isomers).

stations for CBPQT⁴⁺, namely an MPTTF^{15c,18} unit (dark green), a TTF^{15b,d,19} unit (light green), and an oxyphenylene (OP) unit (red). In each case, the dumbbell component is terminated by a diisopropylphenyl (DIPP) stopper^{7e} at one end and a triarylmethyl stopper^{7c,e,14d,17} which is directly connected to the OP unit, at the other end. The TTF and MPTTF units are positioned in the middle of the dumbbell components and are connected by a triethylene glycol (TEG) chain in such a way that the pyrrole moiety of the MPTTF unit points toward the TTF unit in both **1**·4PF₆ and **2**·4PF₆. Based on the three stations' relative affinities toward CBPQT⁴⁺, it is expected that the majority of **1**·4PF₆ and **2**·4PF₆ exist as the translational isomers **1**·MPTTF·4PF₆ and **2**·MPTTF·4PF₆, respectively, in which the CBPQT⁴⁺ ring is located around the MPTTF station (Fig. 1). Subsequently, (ii) the thermodynamic and electrochemical properties of **1**⁴⁺ and **2**⁴⁺ are described, followed by describing (iii) thorough kinetic investigations of the tetra-oxidised [2]rotaxanes **1**⁸⁺ and **2**⁸⁺ using time-resolved ¹H NMR spectroscopy at variable temperatures. Finally, (iv) it is shown that the difference between the size of the TTF²⁺ and the MPTTF²⁺ electrostatic barriers are heavily temperature dependent.

Results and discussion

Synthesis

The [2]rotaxanes **1**·4PF₆ and **2**·4PF₆ were prepared as shown in Schemes S2 and S3 (ESI†). A modular approach was used in which the various parts of the target molecules were prepared individually and joined together in the latter steps of the synthetic pathways to produce the dumbbells **14** and **24**. Formation of the [2]rotaxanes **1**·4PF₆ and **2**·4PF₆ was achieved by using the dumbbells **14** and **24**, respectively, as templates for the formation of the CBPQT⁴⁺ tetracation under high pressure conditions²⁰ from the dicationic precursor²¹ **15**·2PF₆ and the dibromide **16** (see ESI†).

Mass spectrometric investigations

All new compounds reported in this paper were characterised by electrospray ionisation (ESI) mass spectrometry. The ESI mass spectra (Fig. S1 and S2, ESI†) of the [2]rotaxanes **1**·4PF₆ and **2**·4PF₆ revealed peaks corresponding to the doubly positively charged [M – 2PF₆]²⁺ and triply positively charged [M – 3PF₆]³⁺ ions.

Photophysical investigations

The photophysical properties of the dumbbells **14** and **24** and the [2]rotaxanes of **1**⁴⁺ and **2**⁴⁺ were studied in solution at 298 K. The UV/Vis/NIR absorption spectra recorded of **14** (Fig. S3a, ESI†) and **24** (Fig. S3b, ESI†) in MeCN/CH₂Cl₂ only exhibit weak tails in the visible region at λ ≤ 500 nm and both solutions appear yellow. In contrast, solutions of **1**⁴⁺ and **2**⁴⁺ both appear green, and the absorption spectra recorded of **1**⁴⁺ (Fig. S3c, ESI†) and **2**⁴⁺ (Fig. S3d, ESI†) in MeCN showed a broad CT absorption band centered at 807 and 809 nm, respectively, which is characteristic^{7a,15b–d,22} of structures containing a TTF/MPTTF unit positioned inside the cavity of CBPQT⁴⁺. These observations clearly suggest that CBPQT⁴⁺ encircles the rod section of the dumbbell component in the [2]rotaxanes **1**⁴⁺ and **2**⁴⁺ and that either the TTF or the MPTTF unit is located inside the cavity of CBPQT⁴⁺.

¹H NMR spectroscopic investigations

While both mass spectrometry and absorption spectroscopy indicate qualitatively that the CBPQT⁴⁺ ring is present on the rod section of the dumbbell component of **1**⁴⁺ and **2**⁴⁺, ¹H NMR spectroscopy was used as a quantitative tool for monitoring the precise position of CBPQT⁴⁺ on the rod section and hence allowing the relative amounts of the different translational isomers present in **1**⁴⁺ and **2**⁴⁺ to be determined. All of the compounds containing the TTF unit were isolated as mixtures of E/Z isomers on account of the inherent E/Z isomerism of the TTF unit and ¹H NMR spectroscopy confirmed that the ratio between the isomers was approximately 1 : 1 in all cases.

A comparison of the ¹H NMR spectra (400 MHz, CD₃CN, 298 K) of the [2]rotaxane **1**⁴⁺ (Fig. 2) and the dumbbell **14** (Fig. S4, ESI†) revealed new signals resonating at δ = 8.75–9.13 ppm, δ = 7.65–8.13 ppm, δ = 7.65–7.84 ppm and δ = 5.63–5.82 ppm that



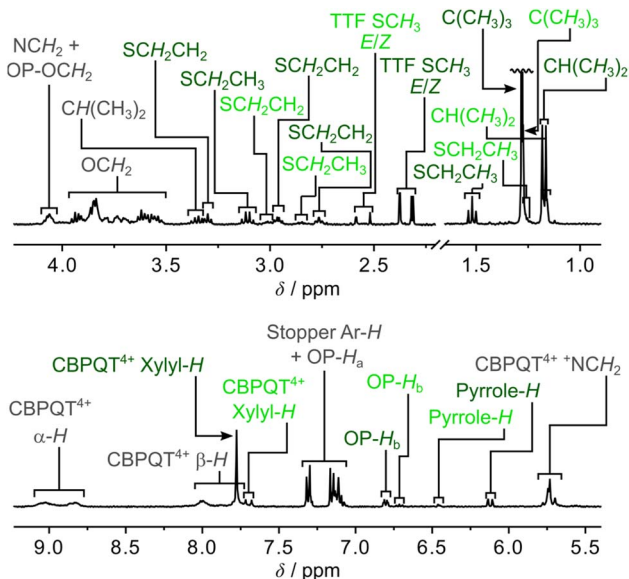


Fig. 2 Partial ^1H NMR spectrum of an isomeric mixture of the [2]rotaxane 1^{4+} (400 MHz, CD_3CN , 298 K, 1.5 mM), where the assignments in light green are associated with $1\cdot\text{TTF}^{4+}$ and the dark green signals are associated with $1\cdot\text{MPTTF}^{4+}$, while the assignments in grey are associated with a mixture of the two translational isomers. The $\text{C}(\text{CH}_3)_3$ signal is not shown in its full height.

can be associated with the $\alpha\text{-H}$, $\beta\text{-H}$, xylyl- H and CH_2N^+ protons, respectively, present in the CBPQT^{4+} ring; this suggests that CBPQT^{4+} is present in 1^{4+} in agreement with the findings obtained from the mass spectrometric and photophysical investigations (*vide supra*).

A careful examination of the ^1H NMR spectrum (400 MHz) of the [2]rotaxane 1^{4+} shows that it exists as a mixture of two stable translational isomers, where CBPQT^{4+} encircles either the TTF (*i.e.* $1\cdot\text{TTF}^{4+}$) or the MPTTF (*i.e.* $1\cdot\text{MPTTF}^{4+}$) station, respectively, and that their exchange is slow on the ^1H NMR timescale (400 MHz) in CD_3CN at 298 K. Thus, several protons in both the dumbbell component and in the CBPQT^{4+} ring gave rise to two sets of signals, one for $1\cdot\text{MPTTF}^{4+}$ and one for $1\cdot\text{TTF}^{4+}$, allowing the population of each of the two translational isomers at equilibrium to be determined. The most diagnostic evidence, which shows that $1\cdot\text{MPTTF}^{4+}$ is present in the isolated mixture is the appearance of an AB system ($J = 1.8$ Hz) at $\delta = 6.11$ and 6.14 ppm, which can be assigned^{7a} to the resonances associated with the two pyrrole- H protons in the MPTTF unit when it is located inside the cavity of CBPQT^{4+} . The resonances for the two pyrrole- H protons in $1\cdot\text{MPTTF}^{4+}$ are upfield shifted as compared to the dumbbell **14**, where they appear at $\delta = 6.62$ –6.67 ppm, a finding that is fully consistent with CBPQT^{4+} encircling the MPTTF unit.^{7a} Furthermore, the two methylene protons of the SEt (SCH_2CH_3) group attached to the MPTTF unit in $1\cdot\text{MPTTF}^{4+}$ are downfield shifted relative to their position in the dumbbell **14** on account of the deshielding effect of CBPQT^{4+} when it encircles the MPTTF unit.^{7c,17} The SCH_2CH_3 protons resonate as a quartet ($J = 7.4$ Hz) at $\delta = 3.11$ ppm in $1\cdot\text{MPTTF}^{4+}$, compared with a quartet ($J = 7.3$ Hz) at $\delta = 2.85$ ppm in the dumbbell **14**. Consistently, the SCH_2 protons

associated with the thioethoxy ($\text{SCH}_2\text{CH}_2\text{O}$) group attached directly to the MPTTF unit in $1\cdot\text{MPTTF}^{4+}$ are similarly shielded and were found (Fig. 2) to resonate as a triplet ($J = 6.3$ Hz) at $\delta = 3.30$ ppm, while the same protons in the dumbbell **14** resonate as a triplet ($J = 6.4$ Hz) at $\delta = 3.01$ ppm. The protons associated with the two thiomethyl (SCH_3) groups, attached to the TTF unit in $1\cdot\text{MPTTF}^{4+}$, gave rise to a total of four singlets resonating at $\delta = 2.31$, 2.32, 2.37 and 2.38 ppm, respectively, and are located at almost identical chemical shift values as in the dumbbell **14** ($\delta = 2.35$, 2.36 and 2.38 ppm).§ The existence of two sets of SCH_3 signals in $1\cdot\text{MPTTF}^{4+}$ at $\delta = 2.31$ and 2.32 ppm and at $\delta = 2.37$ and 2.38 ppm, therefore, indicate that the SCH_3 protons experience two slightly different chemical environments which only can be accounted for by the presence of both an *E*- and a *Z*-isomer in $1\cdot\text{MPTTF}^{4+}$.

The existence of $1\cdot\text{TTF}^{4+}$ is evidenced (Fig. 2) by the presence of three singlets resonating at $\delta = 2.52$, 2.59 and 2.59 ppm,¶ which can be associated with the SCH_3 protons in the *E/Z* isomeric mixture of $1\cdot\text{TTF}^{4+}$. They have experienced a downfield shift relative to the position at which they were found to resonate in the dumbbell **14** ($\delta = 2.35$, 2.36 and 2.38 ppm) and previous investigations^{7c} have shown that such behaviour is entirely consistent with CBPQT^{4+} encircling a TTF unit. The small multiplet centered at $\delta = 6.46$ ppm can be assigned^{14d} to the pyrrole- H protons in the MPTTF unit when the TTF unit is encircled by CBPQT^{4+} . Compared to $1\cdot\text{MPTTF}^{4+}$ ($\delta = 3.11$ ppm), the signal for the SCH_2CH_3 protons in $1\cdot\text{TTF}^{4+}$ ($\delta = 2.85$ ppm) has not been shifted significantly downfield and resonates at almost the same position as the SCH_2CH_3 protons in the dumbbell **14** ($\delta = 2.85$ ppm).

Although the [2]rotaxane 1^{4+} , contains three potential stations for CBPQT^{4+} to reside around, a careful inspection of the ^1H NMR spectrum recorded of 1^{4+} in CD_3CN at 298 K did not show any indication of the presence of the translational isomer where CBPQT^{4+} encircles the OP unit (*i.e.* $1\cdot\text{OP}^{4+}$). Since the [2]rotaxane 1^{4+} , is constructed in such a way that the TTF unit is separated from the OP unit by a combination of an SMe group and a thiotriethylene glycol (TTEG) substituent which is known^{7c,18b} to act as a “speed bump” for CBPQT^{4+} , the shuttling of CBPQT^{4+} between the MPTTF and OP units is expected to be slow on the ^1H NMR timescale. Consequently, if $1\cdot\text{OP}^{4+}$ is present in the isolated mixture of the [2]rotaxane 1^{4+} a third set of signals should appear in the ^1H NMR spectrum. The absence of a signal around 6.25 ppm demonstrates that $1\cdot\text{OP}^{4+}$ is not present in measurable amounts in the isolated mixture of 1^{4+} , since it is known from previous studies^{7c} that the OP-H_a protons resonate as a doublet at $\delta = 6.25$ ppm when the CBPQT^{4+} ring encircles an OP unit in TTF based [2]rotaxanes. Using the integrals of appropriate signals as probes (Table S1, ESI†), the distribution between the two different translational isomers in the [2]rotaxane 1^{4+} can be obtained and it was found that $1\cdot\text{MPTTF}^{4+}$ is the predominant translational isomer, accounting for 82% of the mixture, whereas $1\cdot\text{TTF}^{4+}$ only account for 18% as illustrated in Scheme S2 (ESI†).

As for the [2]rotaxane 1^{4+} , the [2]rotaxane 2^{4+} exists (Fig. S7, ESI†) as a mixture of two interconverting translational isomers (*i.e.* $2\cdot\text{MPTTF}^{4+}$ and $2\cdot\text{TTF}^{4+}$) where their exchange is slow on



the ^1H NMR timescale (400 MHz) in CD_3CN at 298 K. Using a similar analysis (Table S2, ESI†) as carried out on the [2]rotaxane 1^{4+} , it can be estimated that the [2]rotaxane 2^{4+} almost exclusively (95%) exists as the translational isomer $2\cdot\text{MPTTF}^{4+}$ in CD_3CN at 298 K, while $2\cdot\text{TTF}^{4+}$ only is present in tiny amounts (5%) as illustrated in Scheme S3 (ESI†). The presence of $2\cdot\text{MPTTF}^{4+}$ is evidenced (Fig. S7, ESI†) by the characteristic AB system ($J = 2.0$ Hz) resonating at $\delta = 6.17$ and 6.20 ppm assigned to the pyrrole- H protons in the MPTTF unit, when the MPTTF unit is positioned inside CBPQT^{4+} . Furthermore, the existence of $2\cdot\text{MPTTF}^{4+}$ is confirmed by a singlet resonating at $\delta = 2.68$ ppm in the ^1H NMR spectrum of 2^{4+} , which is diagnostic¹⁷ for SCH_3 protons attached to an MPTTF unit when it is encircled by CBPQT^{4+} , while the two small singlets appearing at $\delta = 2.51$ and 2.52 ppm are associated with $2\cdot\text{TTF}^{4+}$ and can be assigned to the SCH_3 protons attached to the TTF unit when it is located inside CBPQT^{4+} . **

To support the experimentally found population of translational isomers in the two [2]rotaxanes, the theoretical distributions of translational isomers were calculated using the binding energies between CBPQT^{4+} and the three different stations, *i.e.* $\Delta G^\circ(\text{MPTTF})^{14d} = -6.0$ kcal mol $^{-1}$, $\Delta G^\circ(\text{TTF})^{7c,14d} = -4.4$ kcal mol $^{-1}$ and $\Delta G^\circ(\text{OP})^{7c} = -1.7$ kcal mol $^{-1}$ in MeCN at 298 K. Assuming that the relative distribution between the translational isomers is related to the above listed binding energies of CBPQT^{4+} with the separate MPTTF, TTF and OP units, it was calculated (see ESI†) that the theoretical distribution between the three translational isomers is 94:6:0 (MPTTF:TTF:OP) in MeCN at 298 K. This is in perfect agreement with the ^1H NMR spectroscopic findings (*vide supra*) which suggest that the proportions of the three translational isomers is 95:5:0 ($2\cdot\text{MPTTF}^{4+}$: $2\cdot\text{TTF}^{4+}$: $2\cdot\text{OP}^{4+}$) for 2^{4+} , while the amount of $1\cdot\text{MPTTF}^{4+}$ compared to the amount of $1\cdot\text{TTF}^{4+}$ in 1^{4+} (82:18:0 ($1\cdot\text{MPTTF}^{4+}$: $1\cdot\text{TTF}^{4+}$: $1\cdot\text{OP}^{4+}$)) is lower than expected from the theoretical calculations. The observed difference in the population of translational isomers in 1^{4+} and 2^{4+} can most likely be accounted for by the fact that the relative position of the stopper groups and the SET/SMe groups along the dumbbell component affects the stability of the different tertiary (3°) structures²³ the two isomeric [2]rotaxanes 1^{4+} and 2^{4+} can adopt in solution.

Electrochemical investigations

The electrochemical properties of the dumbbells **14** and **24** and their corresponding [2]rotaxanes 1^{4+} and 2^{4+} were investigated

using cyclic voltammetry (CV). The cyclic voltammograms (CVs) were all measured in nitrogen-purged MeCN solutions at 298 K, and we have mainly focused our studies on the oxidation processes of the TTF and MPTTF units. The obtained half-wave potentials ($E_{1/2}$) are listed in Table 1, together with the corresponding anodic (E_{ox}) and cathodic (E_{red}) peak potentials.

The CVs of the two isomeric dumbbells **14** and **24** are as expected almost identical (Fig. 3a and b) and show four redox processes. The first redox process appears at $E_{1/2}^1 = 0.00$ V vs. Fc/Fc^+ and can be assigned to the first oxidation of the MPTTF unit ($\text{MPTTF} \rightarrow \text{MPTTF}^{+\cdot}$) to produce $14^{1\cdot/1+}/24^{1\cdot/1+}$, since the MPTTF unit is easier to oxidise than the TTF unit.^{14d,23} Consequently, the second redox process appearing at $E_{1/2}^2 = +0.07/+0.08$ V vs. Fc/Fc^+ can be associated with the first oxidation of the TTF unit ($\text{TTF} \rightarrow \text{TTF}^{+\cdot}$), which will produce $14^{2\cdot/2+}/24^{2\cdot/2+}$. The third and fourth redox processes are observed as two overlapping processes at $E_{1/2}^3 = E_{1/2}^4 = +0.39$ V vs. Fc/Fc^+ and can be attributed to the second oxidations of the MPTTF and TTF units to produce the corresponding dications (*i.e.* $\text{MPTTF}^{+\cdot} \rightarrow \text{MPTTF}^{2+}$ and $\text{TTF}^{+\cdot} \rightarrow \text{TTF}^{2+}$, respectively). As observed previously in similar systems, it seems likely that $\text{MPTTF}^{+\cdot}$ in $14^{2\cdot/2+}/24^{2\cdot/2+}$ will be oxidised at a slightly lower potential relative to $\text{TTF}^{+\cdot}$ to produce initially $14^{1\cdot/3+}/24^{1\cdot/3+}$ followed by the formation of $14^{4+}/24^{4+}$ (Schemes S4 and S5, ESI†).††

In the case of the [2]rotaxanes 1^{4+} and 2^{4+} , a more complex situation occurs, since they both exist as a mixture of two different translational isomers (Schemes S1 and S2, ESI†). However, ^1H NMR spectroscopy revealed (*vide supra*) that the predominant isomer in both cases is the translational isomer in which the CBPQT^{4+} ring encircles the MPTTF unit, *i.e.* $1\cdot\text{MPTTF}^{4+}$ (82%) and $2\cdot\text{MPTTF}^{4+}$ (95%), respectively, and that $1\cdot\text{TTF}^{4+}$ (18%) and $2\cdot\text{TTF}^{4+}$ (5%) are only present in small amounts in 1^{4+} and 2^{4+} , respectively. Thus, the CVs recorded (Fig. 3c and d) of the [2]rotaxanes 1^{4+} and 2^{4+} will provide us with the electrochemical profile of $1\cdot\text{MPTTF}^{4+}$ and $2\cdot\text{MPTTF}^{4+}$, respectively, since it seems reasonable to expect that the two minor isomers (*i.e.* $1\cdot\text{TTF}^{4+}$ and $2\cdot\text{TTF}^{4+}$) only will give rise to small shoulders in the CVs and therefore not interfere to any significant degree with the electrochemical characterisation of $1\cdot\text{MPTTF}^{4+}$ and $2\cdot\text{MPTTF}^{4+}$.

The CVs recorded (Fig. 3c and d) of the [2]rotaxanes 1^{4+} and 2^{4+} are almost identical and the results show that $1\cdot\text{MPTTF}^{4+}$ and $2\cdot\text{MPTTF}^{4+}$ are characterised by four redox processes appearing at the same potentials (Table 1) when errors are taken into account, *i.e.* $E_{1/2} = +0.12, +0.30, +0.38$ and $+0.60$ V vs. Fc/Fc^+

Table 1 Electrochemical data for the dumbbells **14** and **24** together with their corresponding [2]rotaxanes 1^{4+} and 2^{4+} obtained by cyclic voltammetry^a (CV) at 298 K in MeCN (vs. Fc/Fc^+)

Compound	E_{ox}^{1b} [V]	E_{red}^{1c} [V]	$E_{1/2}^{1d}$ [V]	E_{ox}^{2b} [V]	E_{red}^{2c} [V]	$E_{1/2}^{2d}$ [V]	E_{ox}^{3b} [V]	E_{red}^{3c} [V]	$E_{1/2}^{3d}$ [V]	E_{ox}^{4b} [V]	E_{red}^{4c} [V]	$E_{1/2}^{4d}$ [V]
14	+0.02	−0.03	0.00	+0.09	+0.05	+0.07	+0.41	+0.36	+0.39	+0.41	+0.36	+0.39
24	+0.02	−0.03	0.00	+0.10	+0.05	+0.08	+0.41	+0.36	+0.39	+0.41	+0.36	+0.39
1^{4+}	+0.15	+0.08	+0.12	+0.33	+0.28	+0.30	+0.40	+0.35	+0.38	+0.66	+0.54	+0.60
2^{4+}	+0.17	+0.09	+0.13	+0.34	+0.28	+0.31	+0.40	+0.35	+0.38	+0.66	+0.53	+0.60

^a CV measurements of **14**, **24**, 1^{4+} and 2^{4+} in nitrogen-purged solutions (0.5 mM in MeCN (1^{4+} and 2^{4+}) or <0.5 mM in MeCN (**14** and **24**)) were conducted with 0.1 M $n\text{-Bu}_4\text{NPF}_6$ as the electrolyte, a glassy carbon electrode as the working electrode, a Pt counter electrode and a Ag/AgNO_3 reference electrode with a scan rate of 0.1 V s $^{-1}$; E_{ox} , E_{red} and $E_{1/2}$ values vs. Fc/Fc^+ and the estimated errors on the E values are ± 0.01 V.

^b Anodic peak potential. ^c Cathodic peak potential. ^d Half-wave potential, $E_{1/2} = (E_{\text{ox}} + E_{\text{red}})/2$.



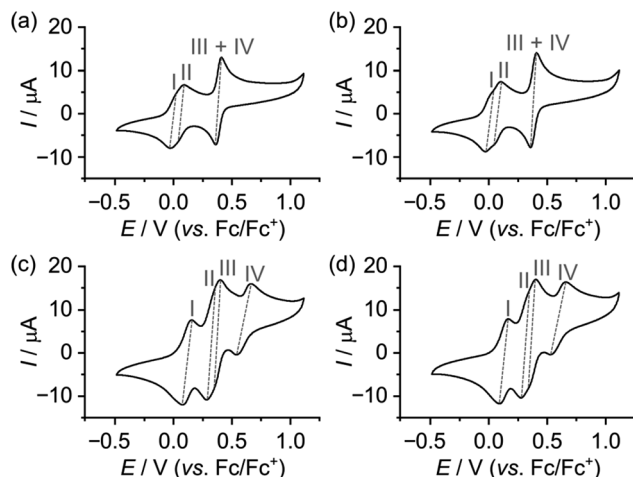


Fig. 3 Cyclic voltammograms of the dumbbells (a) **14** and (b) **24** and the [2]rotaxanes (c) **14**⁺ and (d) **24**⁺. The measurements were carried out at 298 K in nitrogen-purged MeCN solutions (0.5 mM for **14**⁺ and **24**⁺ or <0.5 mM for **14** and **24**) with a glassy carbon electrode as the working electrode, a Pt counter electrode, a Ag/AgNO₃ reference electrode, a scan rate of 0.1 V s⁻¹ and *n*-Bu₄NPF₆ as the electrolyte (0.1 M).

for **1**·MPTTF⁴⁺ and $E_{1/2} = +0.13, +0.31, +0.38$ and $+0.60$ vs. Fc/Fc⁺ for **2**·MPTTF⁴⁺. A suggested mechanism for the four-step oxidation of **1**·MPTTF⁴⁺ is shown in Scheme 2. While the MPTTF unit in the dumbbell **14** (Scheme S4, ESI[†]) was oxidised before the TTF unit, the opposite is observed in the case of **1**·MPTTF⁴⁺. Since the MPTTF unit is located inside the CBPQT⁴⁺ ring in **1**·MPTTF⁴⁺, the first oxidation of the MPTTF unit is expected to occur at a more positive potential ($>+0.30$ V)^{††} compared to the same process in the dumbbell **14** as a result of the strong CT interactions taking place between the MPTTF unit and the bipyridinium moieties in CBPQT⁴⁺. Therefore, the first redox process ($E_{1/2} = +0.12$ V vs. Fc/Fc⁺) of **1**·MPTTF⁴⁺ can be associated with the first oxidation of the TTF unit to TTF^{•+} to give **1**·MPTTF^{1•/5+} (process I, Scheme 2), while the second redox process (process II, Scheme 2) appearing at $E_{1/2} = +0.30$ V vs.

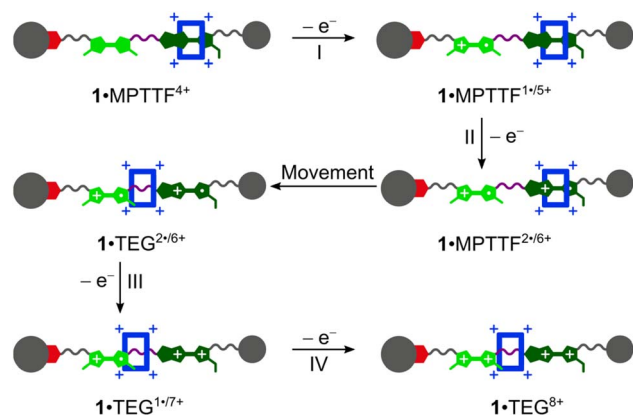
Fc/Fc⁺ can be assigned to the first oxidation of the MPTTF unit encircled by CBPQT⁴⁺ producing **1**·MPTTF^{2•/6+}. A comparison between the third redox process ($E_{1/2}^3$) of the dumbbell **14** ($+0.39$ V vs. Fc/Fc⁺) and the [2]rotaxane **1**·MPTTF⁴⁺ ($+0.38$ V vs. Fc/Fc⁺) reveals that they appear at similar potentials when errors are taken into account. This observation indicates that upon oxidation of MPTTF to MPTTF^{•+} creating **1**·MPTTF^{2•/6+}, the CBPQT⁴⁺ ring will leave the mono-oxidised MPTTF unit on account of coulombic repulsion between the MPTTF^{•+} radical cation and the CBPQT⁴⁺ ring. Since the planar pyrrole moiety (<15 kcal mol⁻¹)^{18b} of the MPTTF unit is a significantly smaller steric barrier than the bulky SET group (>29 kcal mol⁻¹),^{22c} it is evident that the CBPQT⁴⁺ ring is forced to leave the MPTTF^{•+} radical cation *via* the pyrrole-end producing **1**·TEG^{2•/6+} in which the CBPQT⁴⁺ ring is located on the TEG linker in between the TTF^{•+} and MPTTF^{•+} radical cations. As for the dumbbell **14**, it seems likely that the second oxidation of the MPTTF unit in the [2]rotaxane **1**·MPTTF⁴⁺ also will take place before the second oxidation of the TTF unit. Therefore, the third redox process (process III, Scheme 2) appearing at $E_{1/2}^3 = +0.38$ V vs. Fc/Fc⁺ can be assigned to the second oxidation of the MPTTF unit to give **1**·TEG^{1•/7+}. Finally, the fourth redox process observed at $E_{1/2}^4 = +0.60$ V vs. Fc/Fc⁺ can be assigned to the oxidation of the TTF^{•+} radical cation to the TTF²⁺ dication to produce **1**·TEG⁸⁺ (process IV, Scheme 2). Compared to the dumbbell **14**, the $E_{1/2}^4$ value in the [2]rotaxane **1**·MPTTF⁴⁺ is anodically shifted by 0.21 V, a finding which is fully consistent with previous results reported for a tetra-stable [2]rotaxane,^{14d} indicating that the CBPQT⁴⁺ ring upon formation of **1**·TEG^{1•/7+}, is forced to move closer to the TTF^{•+} unit (Scheme 2), which causes the oxidation of TTF^{•+} to TTF²⁺ (*i.e.* process IV) to be more difficult compared to the same process in the dumbbell **14**. These results also show that the CBPQT⁴⁺ ring remains around the TEG linker connecting the TTF and MPTTF units after they have been oxidised on the ~ 20 s timescale of the CV experiment.

A similar analysis can be carried out on the [2]rotaxane **2**·MPTTF⁴⁺ and a suggested mechanism for the four-step oxidation of **2**·MPTTF⁴⁺ is shown in Scheme S6 (ESI[†]).

Chemical oxidation of **14**⁺ and **24**⁺

The outcome of the electrochemical investigations clearly shows that **1**·TEG⁸⁺ and **2**·TEG⁸⁺ were produced upon tetra-oxidation of **1**·MPTTF⁴⁺ and **2**·MPTTF⁴⁺, respectively. Both **1**·TEG⁸⁺ and **2**·TEG⁸⁺ represent out-of-equilibrium²⁴ states of **1**⁸⁺ and **2**⁸⁺, respectively, since the tetracationic CBPQT⁴⁺ ring is pushed into a high energy (metastable) state where it is in an unfavourable position between, and in close proximity to, both a TTF²⁺ and an MPTTF²⁺ dication. Although **1**·TEG⁸⁺ and **2**·TEG⁸⁺ were found to be stable on the short timescale (~ 20 s) of the electrochemical experiments, it is expected that they will relax into more stable translational isomeric forms of **1**⁸⁺ and **2**⁸⁺, respectively, on a longer timescale. For this purpose, ¹H NMR spectroscopy was used to probe the stability of **1**·TEG⁸⁺ and **2**·TEG⁸⁺.

Initially, solutions of the [2]rotaxanes **14**⁺ and **24**⁺ in CD₃CN at 298 K were oxidised with an excess (ten equiv.) of the chemical oxidant tris(4-bromophenyl)ammoniumyl



Scheme 2 Suggested mechanism for tetra-oxidation of **1**·MPTTF⁴⁺ to produce **1**·TEG⁸⁺ in which the CBPQT⁴⁺ ring is located on the TEG linker connecting the TTF²⁺ and MPTTF²⁺ dications.



hexachloroantimonate (TBPASbCl₆). Subsequently, ¹H NMR spectra (400 MHz) were recorded as fast as possible (~5 min) after adding TBPASbCl₆ followed by the recording of ¹H correlation spectroscopy (COSY) spectra. Comparing the ¹H NMR spectra recorded of **1**⁴⁺ at 298 K before (Fig. 2 and 4a) and after oxidation (Fig. 4b) reveals significant shifts to almost all of the signals in both the dumbbell and the ring components, which is consistent with the formation of both the MPTTF²⁺ and TTF²⁺ dications and, hence, the formation of the tetra-oxidised [2]rotaxane **1**⁸⁺. For instance, the signals for the pyrrole-*H* protons attached to the MPTTF unit shift (Fig. 4a) from δ = 6.11 and 6.14 ppm (AB system) for **1**·MPTTF⁴⁺ to δ = 8.02 ppm (singlet) for **1**⁸⁺ (Fig. 4b). Likewise, the protons associated with the two different SCH₃ groups attached to the TTF unit in **1**⁸⁺ are downfield shifted (δ = 2.99 and 3.01 ppm, Fig. 4b) compared to their position in which they are found resonating in the unoxidised [2]rotaxane **1**·MPTTF⁴⁺ (δ = 2.31, 2.32, 2.37 and 2.38 ppm, Fig. 2 and 4a). Previous studies have shown that such behaviour is entirely consistent with the formation of unencircled MPTTF²⁺ and TTF²⁺ dications.^{7c,14d,17,22b,25} Furthermore, the decrease in the number of singlets associated with the SCH₃ protons from four to two, when **1**·MPTTF⁴⁺ is oxidised to **1**⁸⁺, is also consistent with the formation of TTF²⁺ because *E/Z*

isomerism cannot exist once the central double bond of the TTF unit is broken upon oxidation to TTF²⁺. Hence only two SCH₃ signals will be observed in the ¹H NMR spectrum recorded of **1**⁸⁺ at 298 K on account of the non-symmetric structure of the tetra-oxidised dumbbell component.

Secondly, it is also evident from the ¹H NMR spectrum recorded of **1**⁸⁺ at 298 K that **1**⁸⁺ almost exclusively exists as a single translational isomer, namely **1**·OP⁸⁺ in which the CBPQT⁴⁺ ring encircles the OP moiety. The new location of the CBPQT⁴⁺ ring along the dumbbell component of the oxidised [2]rotaxane **1**⁸⁺ is evident from the very large upfield shift (Fig. 4) of the resonances associated with the OP-*H*_a and OP-*H*_b protons (Fig. 1) in the oxidised [2]rotaxane **1**⁸⁺ relative to their positions in **1**·MPTTF⁴⁺. In **1**·MPTTF⁴⁺, the resonances appear (Fig. 2 and 4a) at δ = 7.12 ppm (OP-*H*_a) and δ = 6.80 ppm (OP-*H*_b), while they in **1**⁸⁺ appear (Fig. 4b) at δ = 6.27 ppm (OP-*H*_a) and δ = 2.54 ppm (OP-*H*_b) as a result of the anisotropic shielding effect that occurs when the CBPQT⁴⁺ ring encircles the OP moiety. Consistently, the OCH₂ protons attached directly to the encircled OP moiety in **1**⁸⁺ are also significantly shielded and resonate at δ = 1.42 ppm compared to δ = 4.06 ppm in **1**·MPTTF⁴⁺. Examination of the COSY spectrum for **1**⁸⁺ recorded in CD₃CN at 298 K (Fig. S10, ESI†) clearly shows through-bond scalar

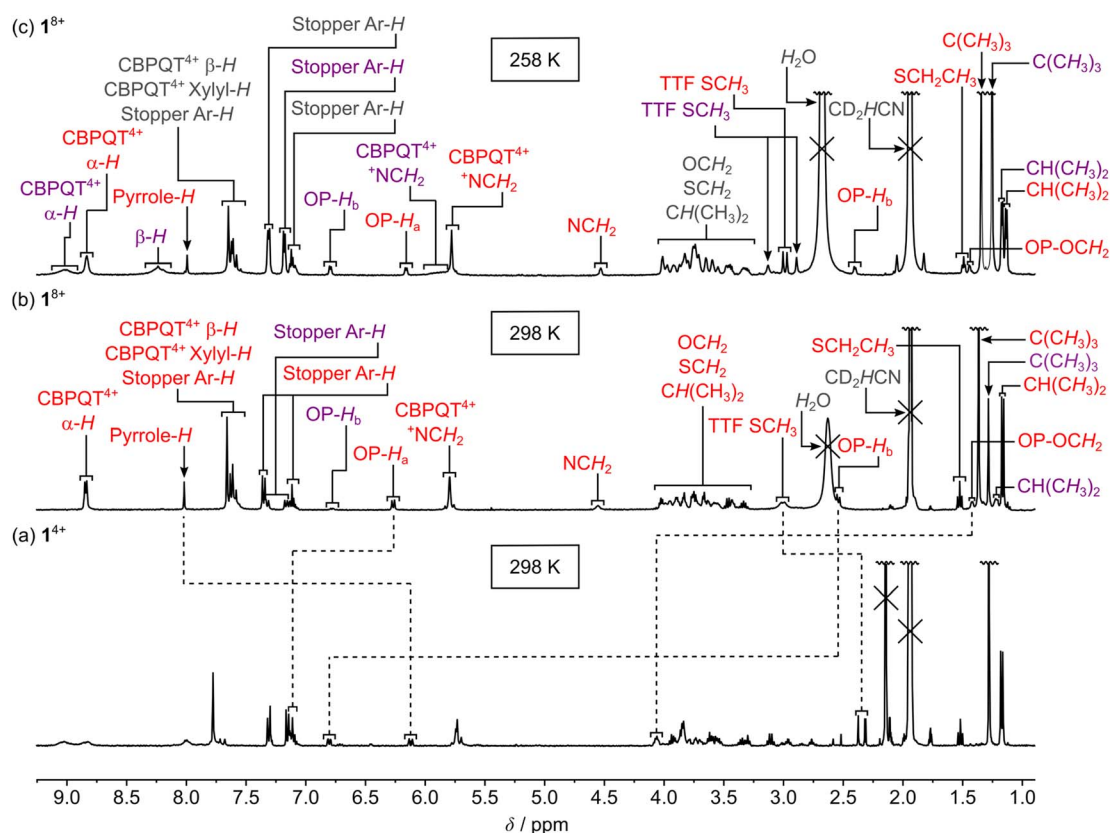


Fig. 4 Partial ¹H NMR spectra (CD₃CN, 1.5 mM) recorded of (a) the [2]rotaxane **1**⁴⁺ (400 MHz) at 298 K, (b) the oxidised [2]rotaxane **1**⁸⁺ (400 MHz) at 298 K and (c) the oxidised [2]rotaxane **1**⁸⁺ (600 MHz) at 258 K. The oxidised [2]rotaxane **1**⁸⁺ was generated by adding an excess of the chemical oxidant tris(4-bromophenyl)ammonium hexachloroantimonate (TBPASbCl₆) to **1**⁴⁺ and the spectra were recorded ca. 5 min after adding TBPASbCl₆ at the indicated temperature. The assignments in red are associated with **1**·OP⁸⁺ (i.e. the OP station is located inside the CBPQT⁴⁺ ring) and the assignments in purple are associated with **1**·TEG⁸⁺ (i.e. the CBPQT⁴⁺ ring is located at the TEG linker connecting the TTF²⁺ and MPTTF²⁺ units). The C(CH₃)₃ and CD₂H₂CN signals are not shown in their full height.



couplings between the two shielded OP- H_a ($\delta = 6.80$ ppm) and OP- H_b ($\delta = 2.54$ ppm) protons and between the OCH₂ ($\delta = 1.42$ ppm) protons attached directly to the encircled OP moiety and the protons in the neighbouring CH₂ ($\delta = 3.46$ ppm) group present in the glycol chain attached to the OP moiety.

Overall, these observations unambiguously confirm that CBPQT⁴⁺ has moved to the OP moiety 5 min after **1**⁴⁺ was oxidised with TBPASbCl₆ at 298 K in CD₃CN and that **1**·TEG⁸⁺ seems to be too short-lived to be observed at 298 K. However, a careful inspection of the ¹H NMR spectrum (Fig. 4b) recorded of **1**⁸⁺ at 298 K, 5 min after being oxidised, reveals signals that cannot be associated with **1**·OP⁸⁺. For example, there is a singlet resonating at $\delta = 1.28$ ppm and a small doublet ($J = 7.8$ Hz) resonating at $\delta = 6.78$ ppm, but in the ¹H NMR spectrum recorded 13 min later (Fig. S9b, ESI†) these signals were almost absent. These results clearly suggest that a dynamic process takes place in the oxidised solution of **1**⁸⁺ and that the decreasing signals appearing at $\delta = 1.28$ ppm and $\delta = 6.78$ ppm most likely can be assigned to the C(CH₃)₃ and OP- H_b protons, respectively, in **1**·TEG⁸⁺.

To reduce the speed in which **1**·TEG⁸⁺ was converted into **1**·OP⁸⁺, a solution of **1**⁴⁺ in CD₃CN was oxidised at a lower temperature (258 K) with an excess of TBPASbCl₆ and once again a ¹H NMR spectrum (400 MHz) was recorded as fast as possible (~5 min) after mixing the two components. In this case, it transpires (Fig. 4c) that both **1**·TEG⁸⁺ and **1**·OP⁸⁺ are present in the oxidised mixture in almost equal proportions, since two sets of distinct signals with equal intensities can be observed in the ¹H NMR spectrum for numerous of the protons present in **1**⁸⁺. For instance, in the aromatic region of the spectrum, two broad signals resonating at $\delta = 8.83$ ppm and $\delta = 9.02$ ppm appear which can be assigned to the bipyridinium α -H protons (Fig. 1) in **1**·OP⁸⁺ and **1**·TEG⁸⁺, respectively. In addition, it is clearly evident from the ¹H NMR spectra recorded of **1**⁸⁺ at 298 K (Fig. 4b) and 258 K (Fig. 4c) that the signal assigned to the OP- H_b protons ($\delta = 6.79$ ppm) in **1**·TEG⁸⁺ has increased in intensity upon lowering the temperature from 298 K to 258 K.

Similar oxidation studies (see ESI†) have been carried out on the [2]rotaxane **2**⁴⁺. In this case, it was found (Fig. S11 and S13b, ESI†) that **2**·OP⁸⁺ was the only translational isomer present at 298 K immediately (~5 min) after **2**·MPTTF⁴⁺ was oxidised with TBPASbCl₆ and that the metastable **2**·TEG⁸⁺ translational isomer only could be observed in significant amounts in the ¹H NMR spectrum (Fig. S13c, ESI†) at lower temperature (253 K).

For both **1**⁸⁺ and **2**⁸⁺, the SET substituent bound to either the MPTTF or the TTF unit, respectively, successfully block the movement of CBPQT⁴⁺ towards the DIPP moiety since no signals in the ¹H NMR spectra that can be associated with CBPQT⁴⁺ encircling the glycol linker attached to the DIPP stopper group were observed.^{7e}

Kinetic investigations of **1**⁸⁺ and **2**⁸⁺

Once the switching mechanism for **1**·MPTTF⁴⁺ and **2**·MPTTF⁴⁺ was established and it qualitatively was found that the metastable translational isomers **1**·TEG⁸⁺ and **2**·TEG⁸⁺ were formed

upon oxidation of **1**·MPTTF⁴⁺ and **2**·MPTTF⁴⁺, respectively, the next step was to monitor the stability of **1**·TEG⁸⁺ and **2**·TEG⁸⁺ by following (Scheme 1) their conversion into the thermodynamically more stable translational isomers **1**·OP⁸⁺ and **2**·OP⁸⁺, respectively. If **1**·TEG⁸⁺ and **2**·TEG⁸⁺ are to be converted into **1**·OP⁸⁺ and **2**·OP⁸⁺, respectively, it requires that the CBPQT⁴⁺ ring moves from its position on the TEG linker between the TTF²⁺ and MPTTF²⁺ dications and over either the TTF²⁺ dication in **1**⁸⁺ or the MPTTF²⁺ dication in **2**⁸⁺ allowing the size of the electrostatic barrier, when CBPQT⁴⁺ moves across one of these two dications, to be quantified.

A series of oxidation experiments were carried out at different temperatures and the conversion of **1**·TEG⁸⁺ and **2**·TEG⁸⁺ into **1**·OP⁸⁺ and **2**·OP⁸⁺, respectively, was monitored using variable temperature (VT) ¹H NMR spectroscopy. The experiments were carried out by preparing stock solutions of the [2]rotaxanes **1**⁴⁺ and **2**⁴⁺ in CD₃CN (1.5 mM) and keeping them at 233 K overnight followed by the addition of an excess of the oxidant TBPASbCl₆ to a sample of the stock solution. Subsequently, ¹H NMR spectra (600 MHz) were recorded as fast as possible after oxidation of **1**⁴⁺ at 243, 253, 258, 263 and 268 K and of **2**⁴⁺ at 243, 253, 263 and 268 K and then approximately every 5 min. Representative examples for **1**⁴⁺ (258 K) and **2**⁴⁺ (253 K) are shown in Fig. S16 (ESI†) and Fig. S17 (ESI†), respectively. It is evident from the time-resolved ¹H NMR spectra that there is a net movement of CBPQT⁴⁺ from the TEG linker (purple) towards the OP unit (red), *i.e.* **1**·TEG⁸⁺ and **2**·TEG⁸⁺ are converted into **1**·OP⁸⁺ and **2**·OP⁸⁺, respectively. These processes are unimolecular reactions and can accordingly be expected to follow first-order kinetics.²⁶ Since the energy of **1**·TEG⁸⁺ and **2**·TEG⁸⁺ are significantly higher than the energy of **1**·OP⁸⁺ and **2**·OP⁸⁺, respectively, it can be assumed that $k_1 \gg k_{-1}$, where k_1 is the rate constant for the movement of CBPQT⁴⁺ from the TEG linker to the OP unit and k_{-1} is the rate constant for the reverse process (Scheme 1). Hence, k_1 can be determined if appropriate data points are collected in the early stage of the experiments where the reverse process is not yet occurring to any significant extent.

The movement of CBPQT⁴⁺ from the TEG linker to the OP unit was followed using several signals associated with protons in both translational isomers as probes (Tables S3 and S4, ESI†). An indicative signal that illustrates this process very well at 253 K is the dominant singlet resonating at 1.25 ppm (Fig. 5b). This signal can be associated with the C(CH₃)₃ protons in **1**·TEG⁸⁺ and it is clearly evident that the intensity of this singlet decreases as a function of time. Concomitant with this change, the intensity of the singlet resonating at 1.34 ppm, which can be assigned to the C(CH₃)₃ protons in **1**·OP⁸⁺, is found to increase over the same time frame illustrating that **1**·TEG⁸⁺ is converted into **1**·OP⁸⁺. In each case, the experimental data were subjected to a first-order analysis, and k_1 values were obtained for the movement of CBPQT⁴⁺ from the TEG linker to the OP unit in CD₃CN at different temperatures. The straight line obtained by plotting $\ln I$ as a function of t , where I is the integral of the signal in question and t is the time, confirmed the first-order nature of the process. Representative examples for the conversion of **1**·TEG⁸⁺ into **1**·OP⁸⁺ and for **2**·TEG⁸⁺ into **2**·OP⁸⁺ are



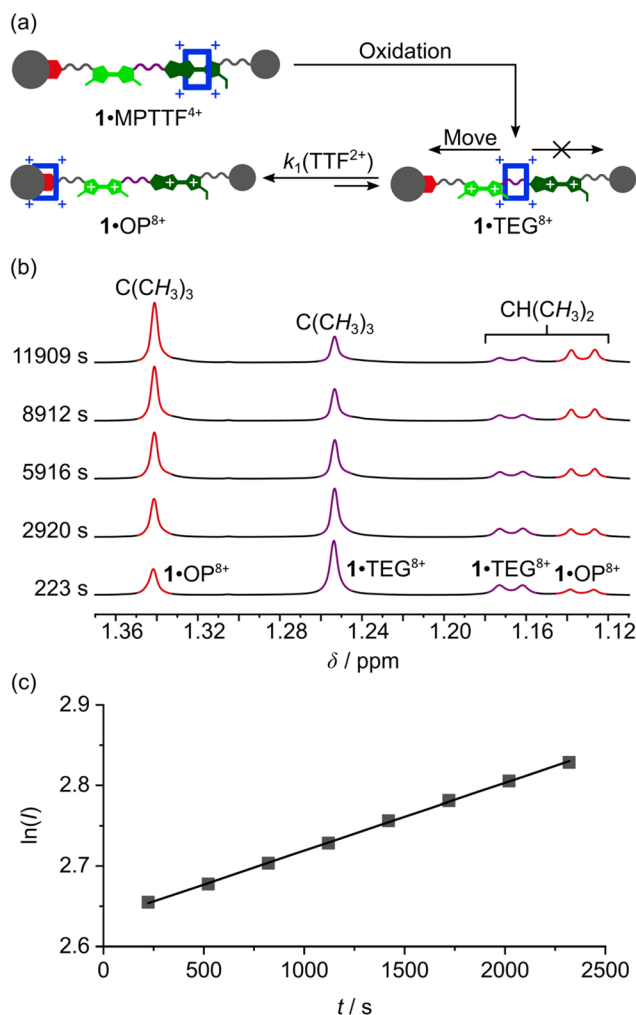


Fig. 5 (a) A cartoon representation illustrating the oxidation of 1-MPTTF⁴⁺ leading initially to the formation of 1-TEG⁸⁺ followed by the movement of CBPQT⁴⁺ across the TTF dication (*i.e.* TTF²⁺) to produce 1-OP⁸⁺. (b) A series of partial ¹H NMR spectra (600 MHz, 253 K, CD₃CN) of the oxidised [2]rotaxane **1**⁸⁺ recorded at different delay times after addition of an excess (28–32 equiv.) of TBPASbCl₆ to **1**⁴⁺ (*c* = 1.5 mM) showing the increasing signals for the resonances associated with the C(CH₃)₃ protons (δ = 1.34 ppm) and the CH(CH₃)₂ protons (δ = 1.13 ppm), respectively, in 1-OP⁸⁺, and the decreasing signals for the resonances associated with the C(CH₃)₃ protons (δ = 1.25 ppm) and the CH(CH₃)₂ protons (δ = 1.17 ppm), respectively, in 1-TEG⁸⁺. (c) Plot of ln *I* against *t* at 253 K for the movement of CBPQT⁴⁺ across the TTF²⁺ unit, where *I* is the integral of the signal at δ = 1.34 ppm. The eight data points have been fitted by the best straight line (black line), giving a correlation coefficient of 1.000, indicating that first-order kinetics are in operation. The slope of the line corresponds to the rate constant *k*₁ for the movement of CBPQT⁴⁺ over the TTF²⁺ unit in **1**⁸⁺, according to the relationship ln *I* = *k*₁*t*.

shown in Fig. 5c and S18c (ESI[†]), respectively. The *k*₁ values and the corresponding free energies of activation ($\Delta G^\ddagger(k_1)$) were obtained directly from the slope of these straight lines and are recorded in Tables S3 and S4 (ESI[†]). Finally, the rate constant (*k*₁^{av}) and the derived energy of activation $\Delta G^\ddagger(k_1^{\text{av}})$ for the movement of CBPQT⁴⁺ from the TEG linker to the OP unit at each temperature were obtained (Table 2) as an average of the *k*₁

Table 2 Average rate constants^a (*k*₁^{av}) and their derived Gibbs free energies of activation^b ($\Delta G^\ddagger(k_1^{\text{av}})$) for the movement of CBPQT⁴⁺ from 1-TEG⁸⁺ to 1-OP⁸⁺ and from 2-TEG⁸⁺ to 2-OP⁸⁺ determined by ¹H NMR spectroscopy (600 MHz) in CD₃CN at different temperatures (*T*)

	<i>T</i> [K]	# probes ^c	<i>n</i> ^d	<i>k</i> ₁ ^{av,e} [$\times 10^{-4}$ s ⁻¹]	$\Delta G^\ddagger(k_1^{\text{av}})^{b,e}$ [kcal mol ⁻¹]
1 ⁸⁺	243	6	6	0.53 ± 0.07	18.90 ± 0.07
	253	10	8	0.81 ± 0.15	19.48 ± 0.10
	258	7	7	1.30 ± 0.10	19.63 ± 0.04
	263	12	5	1.87 ± 0.26	19.83 ± 0.08
	268	13	5	2.40 ± 0.29	20.09 ± 0.07
2 ⁸⁺	243	7	19	0.36 ± 0.03	19.08 ± 0.04
	253	8	9	1.21 ± 0.04	19.28 ± 0.03
	263	15	5	3.43 ± 0.28	19.52 ± 0.05
	268	8	5	5.74 ± 0.43	19.62 ± 0.05

^a The *k*₁^{av} values were obtained by taking the average of the *k*₁ values collected in Tables S3 and S4 (ESI[†]). ^b The $\Delta G^\ddagger(k_1^{\text{av}})$ values were obtained using the relationship $\Delta G^\ddagger = -RT \ln(k_1^{\text{av}} h / k_B T)$ where *R* is the gas constant, *T* is the absolute temperature, *k*₁^{av} is the average rate constant, *h* is Planck's constant and *k*_B is the Boltzmann constant. ^c # probes represent the number of probes used to calculate the average *k*₁^{av}. ^d *n* is the number of data points used to obtain the individual rate constant *k*₁ as described in Tables S3 and S4 (ESI[†]). ^e The errors are calculated from Koumura *et al.*²⁷ with Δt = 0.1 s, ΔT = 0.3 K and ΔI = 5%.

values obtained for each of the different probes collected in Tables S3 and S4 (ESI[†]).

Since the $\Delta G^\ddagger(k_1^{\text{av}})$ values have been determined at different temperatures, the enthalpic ($\Delta H^\ddagger(k_1^{\text{av}})$) and entropic ($\Delta S^\ddagger(k_1^{\text{av}})$) contributions to the processes where 1-TEG⁸⁺ is converted into 1-OP⁸⁺ and 2-TEG⁸⁺ is converted into 2-OP⁸⁺ can be calculated from plots (Fig. 6) of $\Delta G^\ddagger(k_1^{\text{av}})$ against *T*. Straight lines, each with a good fit, can be approximated to the experimental data, and the kinetic parameters obtained from these plots are summarised in Table 3, together with the extrapolated $\Delta G^\ddagger(k_1^{\text{av}})$ values at 298 K. It is evident from inspection of the data in Table 3 that 1-TEG⁸⁺ is converted into 1-OP⁸⁺ more slowly than 2-TEG⁸⁺ is converted into 2-OP⁸⁺ at 298 K. In fact, the Gibbs free energy of activation is 1.2 kcal mol⁻¹ higher in the former than in the latter, indicating that the MPTTF²⁺ dication constitutes a significantly smaller barrier for CBPQT⁴⁺ compared to the TTF²⁺ dication at 298 K. This difference in Gibbs free energy of activation ($\Delta\Delta G^\ddagger$) can be used to describe how CBPQT⁴⁺ will move in the hypothetical [2]rotaxane **R**⁴⁺ (Fig. 7a) following its oxidation to **R**⁸⁺. Structurally, the [2]rotaxane **R**⁴⁺ is very similar to **1**⁴⁺ and **2**⁴⁺, where the only differences are that the DIPP stopper has been replaced by a triarylmethyl stopper connected to an OP unit and that the large bulky SET group has been replaced by a much smaller SME group. In principle, the [2]rotaxane **R**⁴⁺ is tetra-stable, because it is composed of two primary TTF-based stations (*i.e.* TTF and MPTTF) and two identical secondary OP stations. Consequently, it can theoretically exist, as a mixture of four different translational isomers (*i.e.* **R**·OP_{left}⁴⁺, **R**·TTF⁴⁺, **R**·MPTTF⁴⁺ and **R**·OP_{right}⁴⁺), but as in the case of **1**⁴⁺ and **2**⁴⁺, it can be expected that the majority of **R**⁴⁺ will exist as the **R**·MPTTF⁴⁺ translational isomer||| and that **R**·TTF⁴⁺ only will be present in a small amount, while the population of the two OP

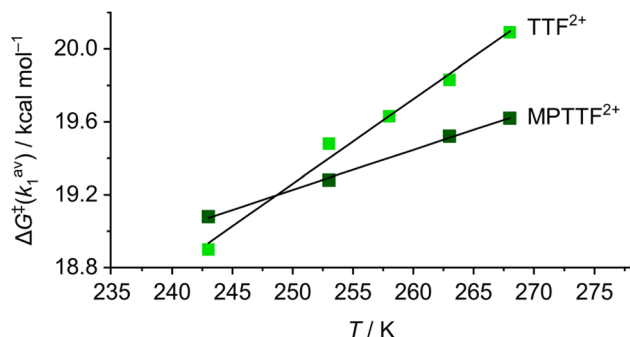


Fig. 6 Linear plots of $\Delta G^\ddagger(k_1^{\text{av}})$ as functions of temperature (T) for the movement of CBPQT^{4+} across either TTF^{2+} (light green points, 1^{8+}) or MPTTF^{2+} (dark green points, 2^{8+}) in CD_3CN . The $\Delta G^\ddagger(k_1^{\text{av}})$ values were obtained as described in Table 2. The data points have been fitted to best straight lines, giving correlation coefficients of 0.982 (1^{8+}) and 0.999 (2^{8+}), respectively. The slope and intercept of each line of best fit give the values $-\Delta S^\ddagger(k_1^{\text{av}})$ and $\Delta H^\ddagger(k_1^{\text{av}})$ (see Table 3), respectively, from the equation $\Delta G^\ddagger(k_1^{\text{av}}) = \Delta H^\ddagger(k_1^{\text{av}}) - T \times \Delta S^\ddagger(k_1^{\text{av}})$.

translational isomers of R^{4+} will be very close to zero. Similar to what is observed for $1 \cdot \text{MPTTF}^{4+}$ and $2 \cdot \text{MPTTF}^{4+}$, oxidation of $\text{R} \cdot \text{MPTTF}^{4+}$ to R^{8+} is expected initially to lead to the formation of the metastable isomer $\text{R} \cdot \text{TEG}^{8+}$ (Fig. 7b), where the CBPQT^{4+} ring is located between the TTF^{2+} and MPTTF^{2+} dications. Since the TTF and MPTTF units in the [2]rotaxane R^{8+} only are substituted with SMe groups, the CBPQT^{4+} ring now has the option to cross either the TTF^{2+} dication or the MPTTF^{2+} dication to produce $\text{R} \cdot \text{OP}^{8+}_{\text{left}}$ or $\text{R} \cdot \text{OP}^{8+}_{\text{right}}$, respectively. Using the $\Delta \Delta G^\ddagger$ value of $1.2 \text{ kcal mol}^{-1}$ (*vide supra*), it can be calculated (see ESI†) that approximately 90% of CBPQT^{4+} will move across the MPTTF^{2+} dication and only 10% over the TTF^{2+} dication when it has the possibility to choose between these two different dications at 298 K.

The fact that the metastable states of the two oxidised [2]rotaxanes (*i.e.* $1 \cdot \text{TEG}^{8+}$ and $2 \cdot \text{TEG}^{8+}$) show (Table 3) significantly different sets of activation parameters ($\Delta G^\ddagger(k_1^{\text{av}})$, $\Delta H^\ddagger(k_1^{\text{av}})$, $\Delta S^\ddagger(k_1^{\text{av}})$) indicates that the rate-limiting steps for the movement of the CBPQT^{4+} ring across the TTF^{2+} and MPTTF^{2+} dications have significantly different qualities. The negative activation entropies observed for both 1^{8+} and 2^{8+} , suggest that there is an increase in the ordering of the transition state structures $1^{8+\ddagger}$ and $2^{8+\ddagger}$ relative to the initial structures of $1 \cdot \text{TEG}^{8+}$ and $2 \cdot \text{TEG}^{8+}$, respectively. In the

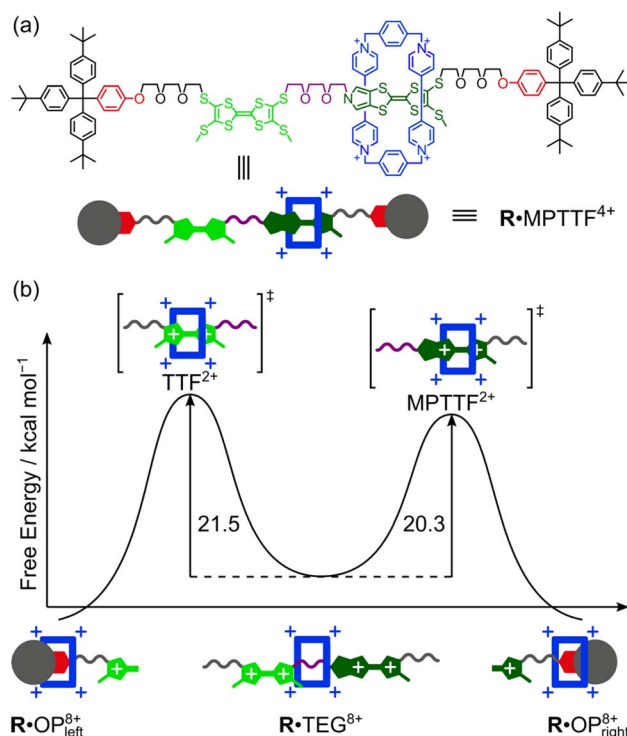


Fig. 7 (a) Molecular formula of the hypothetical tetra-stable [2]rotaxane R^{4+} (only one translational isomer is shown which will exist as a mixture of *E*- and *Z*-isomers) and a cartoon representation of the expected dominating $\text{R} \cdot \text{MPTTF}^{4+}$ translational isomer. (b) Energy diagram showing the Gibbs free energies of activation (ΔG^\ddagger) for the movement of CBPQT^{4+} away from the TEG linker across either a TTF^{2+} dication or an MPTTF^{2+} dication to an OP unit in CD_3CN at 298 K.

[2]rotaxane 1^{8+} , the movement of the CBPQT^{4+} ring from the TEG chain across the TTF^{2+} dication to the OP station has a small enthalpy of activation, $\Delta H^\ddagger(k_1^{\text{av}}) = +7.6 \pm 1.4 \text{ kcal mol}^{-1}$, while the activation entropy is large and negative, $\Delta S^\ddagger(k_1^{\text{av}}) = -46.6 \pm 5.5 \text{ cal mol}^{-1} \text{ K}^{-1}$. The magnitude of this entropic factor is consistent with the need for a significant increase in the ordering of both the SMe group and the TTEG linker to allow passage of the CBPQT^{4+} ring over the SMe/TTEG steric barrier.^{7c} On its way across the SMe/TTEG steric barrier, the CBPQT^{4+} ring is repelled electrostatically by the two positive charges on the TTF^{2+} dication leading to a further decrease in conformational degrees of freedom of

Table 3 Kinetics and associated parameters for the movement of CBPQT^{4+} from $1 \cdot \text{TEG}^{8+}$ across TTF^{2+} to $1 \cdot \text{OP}^{8+}$ and from $2 \cdot \text{TEG}^{8+}$ across MPTTF^{2+} to $2 \cdot \text{OP}^{8+}$ in CD_3CN ^{a,b,c,d,e}

	$k_1^{\text{av}}_{298\text{K}} [\times 10^{-3} \text{ s}^{-1}]$	$t_{1/2}^{\text{av}}_{298\text{K}} [\text{ms}]$	$\Delta G^\ddagger(k_1^{\text{av}})_{298\text{K}} [\text{kcal mol}^{-1}]$	$\Delta H^\ddagger(k_1^{\text{av}}) [\text{kcal mol}^{-1}]$	$\Delta S^\ddagger(k_1^{\text{av}}) [\text{cal mol}^{-1} \text{ K}^{-1}]$
1^{8+}	1.08	0.64	21.5 ± 0.2	7.6 ± 1.4	-46.6 ± 5.5
2^{8+}	8.27	0.08	20.3 ± 0.1	13.7 ± 0.7	-22.0 ± 2.7

^a $k_1^{\text{av}}_{298\text{K}}$, $t_{1/2}^{\text{av}}_{298\text{K}}$, $\Delta G^\ddagger(k_1^{\text{av}})_{298\text{K}}$, $\Delta H^\ddagger(k_1^{\text{av}})$ and $\Delta S^\ddagger(k_1^{\text{av}})$ are the values for the activation parameters. ^b The $\Delta S^\ddagger(k_1^{\text{av}})$ and $\Delta H^\ddagger(k_1^{\text{av}})$ values were obtained from the intercept and slope of the straight line in the plot (Fig. 6) of $\Delta G^\ddagger(k_1^{\text{av}})$ against T using the relationship $\Delta G^\ddagger(k_1^{\text{av}}) = \Delta H^\ddagger(k_1^{\text{av}}) - T \times \Delta S^\ddagger(k_1^{\text{av}})$, where T is the absolute temperature. ^c The $\Delta G^\ddagger(k_1^{\text{av}})_{298\text{K}}$ values were extrapolated from the equation $\Delta G^\ddagger(k_1^{\text{av}}) = \Delta H^\ddagger(k_1^{\text{av}}) - T \times \Delta S^\ddagger(k_1^{\text{av}})$, while the $k_1^{\text{av}}_{298\text{K}}$ values were calculated from the equation $k_1^{\text{av}}_{298\text{K}} = \exp(-\Delta G^\ddagger(k_1^{\text{av}})_{298\text{K}}/RT) \times k_B T/h$. ^d Values for $t_{1/2}^{\text{av}}_{298\text{K}}$ were determined using the equation $t_{1/2}^{\text{av}}_{298\text{K}} = \ln 2/k_1^{\text{av}}_{298\text{K}}$. ^e The errors were calculated from Koumura *et al.*²⁷ with $\Delta t = 0.1 \text{ s}$, $\Delta T = 0.3 \text{ K}$ and $\Delta I = 5\%$.



the transition state structure. Once the CBPQT⁴⁺ ring has managed to get over the first SMe/TTEG steric barrier and now encircles the TTF²⁺ dication, it seems likely that the energy for the movement of CBPQT⁴⁺ over the second SMe/TTEG steric barrier will be smaller, because of the large electrostatic repulsion between CBPQT⁴⁺ and the TTF²⁺ dication. By contrast, the [2]rotaxane **2**⁸⁺ shows an overall activation barrier that is enthalpic in nature ($\Delta H^\ddagger(k_1^{\text{av}}) = +13.7 \pm 0.7 \text{ kcal mol}^{-1}$) with a much reduced entropic contribution ($\Delta S^\ddagger(k_1^{\text{av}}) = -22.0 \pm 2.7 \text{ cal mol}^{-1} \text{ K}^{-1}$). The large activation enthalpy observed in the [2]rotaxane **2**⁸⁺ can most likely be accounted for by the fact that the CBPQT⁴⁺ ring needs to move across the MPTTF²⁺ dication (electrostatic barrier) leading to an increase in enthalpy before it is forced to move over the SMe/TTEG steric barrier. Since the MPTTF unit only is attached to one SMe group and is more elongated compared to the TTF unit, the transition state structure of **2**⁸⁺ is most likely less ordered and consequently has lower entropic contribution relative to the transition state structure of **1**⁸⁺.

Finally, it is evident from Fig. 6 and Table 3 that the size of the TTF²⁺ and the MPTTF²⁺ electrostatic activation barriers are heavily temperature dependent. At high temperatures ($T > 298 \text{ K}$), the MPTTF²⁺ dication constitutes a significantly smaller barrier for CBPQT⁴⁺ compared to the TTF²⁺ dication, while the reverse is true at low temperature ($T < 200 \text{ K}$). This observation demonstrates that temperature potentially can be used to control in which direction the CBPQT⁴⁺ ring will move upon oxidation of MIMs incorporating both a TTF and an MPTTF unit.

Conclusions

In conclusion, the syntheses of two isomeric tri-stable [2]rotaxanes **1**·4PF₆ and **2**·4PF₆, with three different stations, a tetrathiafulvalene (TTF), a monopyrrolotetrathiafulvalene (MPTTF) and an oxyphenylene (OP) unit, for the tetracationic cyclobis(paraquat-*p*-phenylene) (CBPQT⁴⁺) ring have been reported. In both cases, ¹H NMR spectroscopic analysis revealed that the [2]rotaxanes exist primarily as the translational isomer in which CBPQT⁴⁺ encircles the MPTTF station (*i.e.* **1**·MPTTF⁴⁺ and **2**·MPTTF⁴⁺). Following tetra-oxidation of **1**·MPTTF⁴⁺ and **2**·MPTTF⁴⁺, either electrochemically or chemically, it was found that a metastable state was formed in which the CBPQT⁴⁺ ring was located on the triethylene (TEG) glycol linker connecting the TTF²⁺ and MPTTF²⁺ dications producing **1**·TEG⁸⁺ and **2**·TEG⁸⁺, respectively. The steric hindrance exhibited from the SET group situated on either the MPTTF unit in **1**·TEG⁸⁺ or the TTF unit in **2**·TEG⁸⁺ made it possible to study the kinetics when these high-energy co-conformations slowly interconvert into thermodynamically more stable co-conformations (*i.e.* **1**·OP⁸⁺ and **2**·OP⁸⁺). The conversion could be followed by ¹H NMR spectroscopy at different temperatures allowing us to calculate the rate constants and associated energies of activation. From our kinetic studies, we were able to determine the free energy of the transition state when CBPQT⁴⁺ moves across either a TTF²⁺ (21.5 kcal mol⁻¹) or an MPTTF²⁺ (20.3 kcal mol⁻¹) electrostatic barrier at 298 K. Consequently, it can be concluded that the TTF²⁺ dication constitutes

a significantly higher electrostatic barrier for CBPQT⁴⁺ compared to the MPTTF²⁺ dication at 298 K. In fact, the Gibbs free energy of activation is 1.2 kcal mol⁻¹ higher in the former than in the latter showing that approximately 90% of CBPQT⁴⁺ will move across the MPTTF²⁺ dication and only 10% over the TTF²⁺ dication when it has the possibility to choose between these two different dications. Furthermore, the electrostatic barrier for the movement of CBPQT⁴⁺ across the MPTTF²⁺ (20.3 kcal mol⁻¹) dication in the tetra-oxidised [2]rotaxane **2**⁸⁺ is 1.5 kcal mol⁻¹ smaller compared to the movement of CBPQT⁴⁺ across a similar MPTTF²⁺ (21.8 kcal mol⁻¹) dication in a bistable [2]rotaxane^{7e} containing only an MPTTF unit in the dumbbell component. This observation can be accounted for by the increased electrostatic repulsion present when the CBPQT⁴⁺ ring is located between two doubly oxidised units (*i.e.* TTF²⁺ and MPTTF²⁺) in **2**⁸⁺. Our results demonstrate for the first time that the combination of a TTF and an MPTTF unit following their oxidations can be used to induce directional movement of the CBPQT⁴⁺ ring in molecular machines with a 90% efficiency – a feature that might be used to construct an electroactive pumping unit that works under oxidative conditions allowing rotaxanes and catenanes incorporating TTF and MPTTF to be designed which show electrically driven unidirectional motion, *i.e.* rotary and linear molecular motors.

Data availability

Synthetic procedures and characterisation data along with the kinetic data are available in the ESI.†

Author contributions

Conceptualisation and methodology: RF, MLS and JOJ. SKJ and MLS performed the synthesis with contributions from MCL and SEW. Investigation: SKJ performed the described investigations of the two [2]rotaxanes with supervision by RF and JOJ. Writing: SKJ, MSN, RF and JOJ prepared the original manuscript with revisions made by SKJ, MSN and JOJ.

Conflicts of interest

There are no conflicts to declare.

Acknowledgements

This work was supported by the Independent Research Fund Denmark | Natural Sciences (FNU, project no. 9040-00169B) and the Villum Foundation.

Notes and references

‡ The combination of an SMe and an SR group constitutes a larger barrier for the CBPQT⁴⁺ ring than the pyrrole moiety which results in CBPQT⁴⁺ initially moving across the pyrrole moiety upon oxidation of the MPTTF unit.^{7e}

§ In the dumbbell **14**, the SCH₃ protons only give rise to three singlets, most likely because of overlap between two of the four singlets, which is supported by the fact that one of the observed singlets resonating at $\delta = 2.36 \text{ ppm}$ is twice as intense as the other two singlets resonating at $\delta = 2.35$ and 2.38 ppm .



¶ As for the dumbbell **14**, the SCH_3 protons in $1\cdot\text{TTF}^{4+}$ only give rise to three singlets, because of overlap between two of the four singlets, supported by the fact that one of the observed singlets resonating at $\delta = 2.52$ ppm is twice as intense as the other two singlets.

|| A comparison of the ^1H NMR spectra (400 MHz) recorded of the dumbbell **24** (Fig. S6†) and the [2]rotaxane 2^{4+} (Fig. S7†) in CD_3CN at 298 K, reveals that the pyrrole- H protons in $2\cdot\text{MPTTF}^{4+}$ have been upfield shifted compared to the dumbbell **24**, where they resonate as a singlet at $\delta = 6.63$ ppm.

** The existence of two SCH_3 signals for $2\cdot\text{TTF}^{4+}$ indicates that it exists as a mixture of E - and Z -isomers.

†† It has previously been shown by the use of appropriate MPTTF and TTF model compounds that both the first ($\Delta E_{1/2}^1 = -0.08$ V) and the second ($\Delta E_{1/2}^2 = -0.02$ V) oxidation process associated with the MPTTF unit take place at potentials that are less positive than those observed for the TTF unit.^{14d}

‡‡ In a single-station [2]rotaxane, containing an MPTTF station in the dumbbell component and CBPQT $^{4+}$ as the ring component, the first redox-wave was shifted 0.33 V toward a more positive potential, compared to the same process in the corresponding dumbbell.^{7a}

§§ Upon oxidation of 1^{4+} , the small amount (18%) of $1\cdot\text{TTF}^{4+}$, present in the isomeric mixture of 1^{4+} will also be oxidised and converted either into $1\cdot\text{TEG}^{8+}$ or directly into $1\cdot\text{OP}^{8+}$.

¶¶ At each temperature and for each probe, first-order kinetics are observed to be in operation, i.e. good straight lines are observed (see Tables S3 and S4, ESI†) when $\ln I$ is plotted against t , where I is the integral of the signal in question and t is the time. This outcome is a consequence of the fact that the data points were collected in the early stage of the experiments where the reverse process is not yet occurring to any significant extent (see ESI†).

||| It should be emphasised that $\text{R}\cdot\text{MPTTF}^{4+}$ has not yet been synthesised, but only represents a model compound used to illustrate how much CBPQT $^{4+}$ will move across an MPTTF $^{2+}$ dication compared to a TTF $^{2+}$ dication when they both are substituted with SMe groups.

- (a) Ó. Gutiérrez-Sanz, P. Natale, I. Márquez, M. C. Marques, S. Zacarias, M. Pita, I. A. C. Pereira, I. López-Montero, A. L. De Lacey and M. Vélez, *Angew. Chem., Int. Ed.*, 2016, **55**, 6216–6220; (b) S. Mukherjee and A. Warshel, *Photosynth. Res.*, 2017, **134**, 1–15.
- (a) S. Liepelt and R. Lipowsky, *Phys. Rev. Lett.*, 2007, **98**, 258102; (b) M. Von Delius, E. M. Geertsema and D. A. Leigh, *Nat. Chem.*, 2010, **2**, 96–101; (c) M. L. Mugnai, C. Hyeon, M. Hinczewski and D. Thirumalai, *Rev. Mod. Phys.*, 2020, **92**, 025001.
- S. Erbas-Cakmak, D. A. Leigh, C. T. McTernan and A. L. Nussbaumer, *Chem. Rev.*, 2015, **115**, 10081–10206.
- E. R. Kay, D. A. Leigh and F. Zerbetto, *Angew. Chem., Int. Ed.*, 2007, **46**, 72–191.
- (a) S. Kassem, T. Van Leeuwen, A. S. Lubbe, M. R. Wilson, B. L. Feringa and D. A. Leigh, *Chem. Soc. Rev.*, 2017, **46**, 2592–2621; (b) S. Erbas-Cakmak, S. D. P. Fielden, U. Karaca, D. A. Leigh, C. T. McTernan, D. J. Tetlow and M. R. Wilson, *Science*, 2017, **358**, 340–343; (c) L. Zhang, V. Marcos and D. A. Leigh, *Proc. Natl. Acad. Sci. U. S. A.*, 2018, **115**, 9397–9404; (d) Y. Qiu, Y. Feng, Q.-H. Guo, R. D. Astumian and J. F. Stoddart, *Chem*, 2020, **6**, 1952–1977; (e) M. N. Tasbas, E. Sahin and S. Erbas-Cakmak, *Coord. Chem. Rev.*, 2021, **443**, 214039; (f) A. Mondal, R. Toyoda, R. Costil and B. L. Feringa, *Angew. Chem., Int. Ed.*, 2022, **61**, e202206631; (g) S. Borsley, E. Kreidt, D. A. Leigh and B. M. W. Roberts, *Nature*, 2022, **604**, 80–85; (h) L. Zhang, Y. Qiu, W.-G. Liu, H. Chen, D. Shen, B. Song, K. Cai, H. Wu, Y. Jiao, Y. Feng, J. S. W. Seale, C. Pezzato, J. Tian, Y. Tan, X.-Y. Chen, Q.-H. Guo, C. L. Stern, D. Philp, R. D. Astumian, W. A. Goddard III and J. F. Stoddart, *Nature*, 2023, **613**, 280–286.
- N. Koumura, R. W. J. Zijlstra, R. A. Van Delden, N. Harada and B. L. Feringa, *Nature*, 1999, **401**, 152–155.
- (a) J. O. Jeppesen, K. A. Nielsen, J. Perkins, S. A. Vignon, A. Di Fabio, R. Ballardini, M. T. Gandolfi, M. Venturi, V. Balzani, J. Becher and J. F. Stoddart, *Chem.-Eur. J.*, 2003, **9**, 2982–3007; (b) J. D. Badjic, V. Balzani, A. Credi, S. Silvi and J. F. Stoddart, *Science*, 2004, **303**, 1845–1849; (c) S. S. Andersen, A. I. Share, B. L. C. Poulsen, M. Körner, T. Duedal, C. R. Benson, S. W. Hansen, J. O. Jeppesen and A. H. Flood, *J. Am. Chem. Soc.*, 2014, **136**, 6373–6384; (d) M. R. Wilson, J. Solà, A. Carlone, S. M. Goldup, N. Lebrasseur and D. A. Leigh, *Nature*, 2016, **534**, 235–240; (e) M. S. Neumann, A. F. Smith, S. K. Jensen, R. Frederiksen, M. L. Skavenborg and J. O. Jeppesen, *Chem. Commun.*, 2023, **59**, 6335–6338.
- C. J. Bruns and J. F. Stoddart, *The Nature of the Mechanical Bond: From Molecules to Machines*, John Wiley & Sons, Inc., Hoboken, New Jersey, 2016.
- J. W. Steed and J. L. Atwood, *Supramolecular Chemistry*, John Wiley & Sons Ltd, Chippingham, Wiltshire, 2nd edn, 2009.
- (a) M. N. Chatterjee, E. R. Kay and D. A. Leigh, *J. Am. Chem. Soc.*, 2006, **128**, 4058–4073; (b) J. S. W. Seale, Y. Feng, L. Feng, R. D. Astumian and J. F. Stoddart, *Chem. Soc. Rev.*, 2022, **51**, 8450–8475.
- R. D. Astumian, *Nat. Commun.*, 2019, **10**, 3837.
- (a) C. Cheng, P. R. McGonigal, S. T. Schneebeli, H. Li, N. A. Vermeulen, C. Ke and J. F. Stoddart, *Nat. Nanotechnol.*, 2015, **10**, 547–553; (b) C. Pezzato, M. T. Nguyen, C. Cheng, D. J. Kim, M. T. Otley and J. F. Stoddart, *Tetrahedron*, 2017, **73**, 4849–4857.
- L. M. Zhao, L. S. Zheng, X. Wang and W. Jiang, *Angew. Chem., Int. Ed.*, 2022, **61**, e202214296.
- (a) A. C. Fahrenbach, Z. Zhu, D. Cao, W.-G. Liu, H. Li, S. K. Dey, S. Basu, A. Trabolsi, Y. Y. Botros, W. A. Goddard III and J. F. Stoddart, *J. Am. Chem. Soc.*, 2012, **134**, 16275–16288; (b) H. V. Schröder and C. A. Schalley, *Beilstein J. Org. Chem.*, 2018, **14**, 2163–2185; (c) S. S. Andersen, A. W. Saad, R. Kristensen, T. S. Pedersen, L. J. O'Driscoll, A. H. Flood and J. O. Jeppesen, *Org. Biomol. Chem.*, 2019, **17**, 2432–2441; (d) M. Jensen, R. Kristensen, S. S. Andersen, D. Bendixen and J. O. Jeppesen, *Chem.-Eur. J.*, 2020, **26**, 6165–6175; (e) X. Y. Chen, H. Chen and J. Fraser Stoddart, *Angew. Chem., Int. Ed.*, 2022, **62**, e202211387.
- (a) D. Philp, A. M. Z. Slawin, N. Spencer, J. F. Stoddart and D. J. Williams, *J. Chem. Soc., Chem. Commun.*, 1991, 1584–1586; (b) W. Devonport, M. A. Blower, M. R. Bryce and L. M. Goldenberg, *J. Org. Chem.*, 1997, **62**, 885–887; (c) J. O. Jeppesen, J. Perkins, J. Becher and J. F. Stoddart, *Org. Lett.*, 2000, **2**, 3547–3550; (d) M. B. Nielsen, J. O. Jeppesen, J. Lau, C. Lomholt, D. Damgaard, J. P. Jacobsen, J. Becher and J. F. Stoddart, *J. Org. Chem.*, 2001, **66**, 3559–3563.
- M. Asakawa, P. R. Ashton, V. Balzani, A. Credi, C. Hamers, G. Mattersteig, M. Montalti, A. N. Shipway, N. Spencer,



- J. F. Stoddart, M. S. Tolley, M. Venturi, A. J. P. White and D. J. Williams, *Angew. Chem., Int. Ed.*, 1998, **37**, 333–337.
- 17 R. Kristensen, M. S. Neumann, S. S. Andersen, P. C. Stein, A. H. Flood and J. O. Jeppesen, *Org. Biomol. Chem.*, 2022, **20**, 2233–2248.
- 18 (a) J. O. Jeppesen, J. Becher and J. F. Stoddart, *Org. Lett.*, 2002, **4**, 557–560; (b) J. O. Jeppesen, S. A. Vignon and J. F. Stoddart, *Chem.–Eur. J.*, 2003, **9**, 4611–4625; (c) R. Kristensen, S. S. Andersen, G. Olsen and J. O. Jeppesen, *J. Org. Chem.*, 2017, **82**, 1371–1379.
- 19 (a) Z.-T. Li, P. C. Stein, N. Svenstrup, K. H. Lund and J. Becher, *Angew. Chem., Int. Ed. Engl.*, 1995, **34**, 2524–2528; (b) P. R. Ashton, V. Balzani, J. Becher, A. Credi, M. C. T. Fyfe, G. Mattersteig, S. Menzer, M. B. Nielsen, F. M. Raymo, J. F. Stoddart, M. Venturi and D. J. Williams, *J. Am. Chem. Soc.*, 1999, **121**, 3951–3957.
- 20 F.-G. Klärner and F. Wurche, *J. Prakt. Chem.*, 2000, **342**, 609–636.
- 21 P. L. Anelli, P. R. Ashton, R. Ballardini, V. Balzani, M. Delgado, M. T. Gandolfi, T. T. Goodnow, A. E. Kaifer, D. Philp, M. Pietraszkiewicz, L. Prodi, M. V. Reddington, A. M. Z. Slawin, N. Spencer, J. F. Stoddart, C. Vicent and D. J. Williams, *J. Am. Chem. Soc.*, 1992, **114**, 193–218.
- 22 (a) J. O. Jeppesen, J. Perkins, J. Becher and J. F. Stoddart, *Angew. Chem., Int. Ed.*, 2001, **40**, 1216–1221; (b) J. O. Jeppesen, S. Nygaard, S. A. Vignon and J. F. Stoddart, *Eur. J. Org. Chem.*, 2005, 196–220; (c) S. Nygaard, B. W. Laursen, A. H. Flood, C. N. Hansen, J. O. Jeppesen and J. F. Stoddart, *Chem. Commun.*, 2006, 144–146; (d) S. Nygaard, K. C. F. Leung, I. Aprahamian, T. Ikeda, S. Saha, B. W. Laursen, S.-Y. Kim, S. W. Hansen, P. C. Stein, A. H. Flood, J. F. Stoddart and J. O. Jeppesen, *J. Am. Chem. Soc.*, 2007, **129**, 960–970; (e) S. S. Andersen, M. Jensen, A. Sørensen, E. Miyazaki, K. Takimiya, B. W. Laursen, A. H. Flood and J. O. Jeppesen, *Chem. Commun.*, 2012, **48**, 5157–5159.
- 23 S. W. Hansen, P. C. Stein, A. Sørensen, A. I. Share, E. H. Witlicki, J. Kongsted, A. H. Flood and J. O. Jeppesen, *J. Am. Chem. Soc.*, 2012, **134**, 3857–3863.
- 24 (a) J. H. Van Esch, R. Klajn and S. Otto, *Chem. Soc. Rev.*, 2017, **46**, 5474–5475; (b) R. Merindol and A. Walther, *Chem. Soc. Rev.*, 2017, **46**, 5588–5619; (c) S. A. P. Van Rossum, M. Tena-Solsona, J. H. Van Esch, R. Eelkema and J. Boekhoven, *Chem. Soc. Rev.*, 2017, **46**, 5519–5535; (d) J. Matern, Y. Dorca, L. Sánchez and G. Fernández, *Angew. Chem., Int. Ed.*, 2019, **58**, 16730–16740.
- 25 S. Nygaard, Y. Liu, P. C. Stein, A. H. Flood and J. O. Jeppesen, *Adv. Funct. Mater.*, 2007, **17**, 751–762.
- 26 K. J. Laidler, *Chemical Kinetics*, Harper Collins, New York, 1987.
- 27 N. Koumura, E. M. Geertsema, M. B. Van Gelder, A. Meetsma and B. L. Feringa, *J. Am. Chem. Soc.*, 2002, **124**, 5037–5051.

